

Silver nanoparticle facilitated charge generation in tandem organic light-emitting devices

Fei Yan, Rui Chen, H. D. Sun, and Xiao Wei Sun

Citation: *Appl. Phys. Lett.* **102**, 203303 (2013); doi: 10.1063/1.4807664

View online: <http://dx.doi.org/10.1063/1.4807664>

View Table of Contents: <http://apl.aip.org/resource/1/APPLAB/v102/i20>

Published by the [American Institute of Physics](#).

Additional information on *Appl. Phys. Lett.*

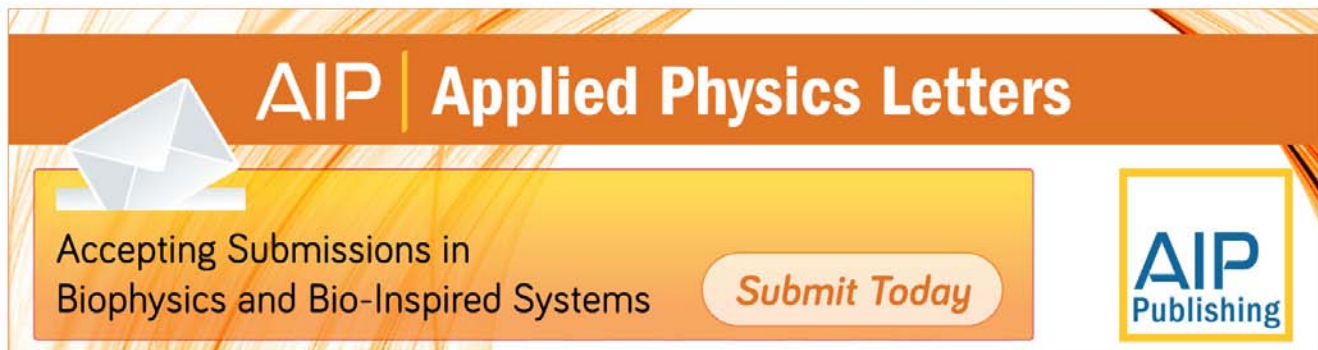
Journal Homepage: <http://apl.aip.org/>

Journal Information: http://apl.aip.org/about/about_the_journal

Top downloads: http://apl.aip.org/features/most_downloaded

Information for Authors: <http://apl.aip.org/authors>

ADVERTISEMENT



AIP | Applied Physics Letters

Accepting Submissions in
Biophysics and Bio-Inspired Systems

Submit Today

AIP
Publishing

Silver nanoparticle facilitated charge generation in tandem organic light-emitting devices

Fei Yan,¹ Rui Chen,² H. D. Sun,² and Xiao Wei Sun^{1,3,a)}

¹LUMINOUS! Center of Excellence for Semiconductor Lighting and Displays, School of Electrical and Electronic Engineering, Nanyang Technological University, 50 Nanyang Avenue, Singapore 639798

²Division of Physics and Applied Physics, School of Physical and Mathematical Sciences Nanyang Technological University, Singapore 637371

³South University of Science and Technology, 1088 Xue-Yuan Road, Shenzhen, Guangdong 518055, China

(Received 5 March 2013; accepted 7 May 2013; published online 22 May 2013)

By inserting an ultrathin silver nanoparticles (Ag NPs) layer between n- and p-type layer of charge generation connector, the performance of the tandem organic light emitting device was improved drastically; the driving voltage was lowered and the luminous efficiency was increased significantly. As the common electrode for two emissive units, Ag NP layer sits at the PN heterojunction interface responsible for charge generation and offers more charge carriers under a lower driving voltage. Additionally, the surface plasmonic resonance of Ag NPs also plays an important role on device improvement. © 2013 AIP Publishing LLC. [<http://dx.doi.org/10.1063/1.4807664>]

Organic light-emitting diodes (OLEDs) are current-driven devices. Ideally, their luminance should linearly increase with the increasing current density. However, to achieve higher luminance in an actual application, an OLED has to operate at a relatively high current density, which induces severe bi-exciton,¹ polaron-exciton annihilation,² and Joule heating,³ undesirably leading to a lower efficiency level and a shorter operational lifetime. By connecting two or more emissive units in series, the so-called tandem OLEDs offer the capability of higher current efficiency levels, longer operational lifetimes, and higher brightness compared to a single emissive unit OLED, while maintaining the same current density as the single unit OLED.⁴⁻⁷ In general, to make a low driving voltage and high efficiency tandem device, an excellent connector prone to generate charge is required.⁵⁻¹⁰

Similar with P and N doped charge injection layers, for p-type layer used in the charge generation layer (CGC), molecules or transition metal oxides with high electron affinity are excellent dopant, such as 2,3,5,6-tetrafluoro-7,7,8,8-tetracyanoquinodimethane (F4-TCNQ),⁹ molybdenum oxide (MoO₃),^{9,10} and tungsten oxide (WO₃).^{8,10} For n-type layer, chemicals with low ionization potential are required. So far, mostly used n-type dopant are active metals (such as magnesium,⁸ cesium,⁴ and lithium^{9,10}), active metal-salt compounds (such as cesium carbonate, Cs₂CO₃),⁶ and some special organic molecule dopants. The cesium and lithium metals are difficult to handle and store because of their activity. And their atoms are small in size and easy to diffuse into emission region, quenching the electroluminescence (EL).¹¹ Additionally, the chamber contamination is also a problem for magnesium evaporation. For organic n-type dopants, besides their expensive prices, we hardly know anything from vendors.

Considering all these features, among all n-type dopants, Cs₂CO₃ is a good choice, which shows excellent electron injection for cathode ohmic contact in single emissive unit devices. But it is not so good to be used in the CGC in

tandem devices.^{6,12,13} In this work, to show the effect of silver, we selected Cs₂CO₃ as the dopant and 2,2',2''-(1,3,5-benzinetriyl)-tris(1-phenyl-1-H-benzimidazole) (TPBi) as host for n-type layer in the CGC. A classical combination of F4-TCNQ doped 4,4',4''-tris(N-3-methylphenyl-N-phenyl-mino)triphenylamine (m-MTDATA) served as p-type layer.^{14,15} The control device is with such n- and p-type layers.

Five OLEDs were fabricated and compared: Device-A: ITO/m-MTDATA (40 nm)\N,N'-di(naphthalene-1-yl)-N,N'-diphenyl-benzidine (NPB) (10 nm)\4,4',4''-tris(carbazol-9-yl)triphenylamine (TcTa) (10 nm)\TcTa:TPBi:Bis(3,5-difluoro-2-(2-pyridyl)phenyl-(2-arboxypyridyl)iridium(III)) (FIRPic) (1:1 7 wt. %, 20 nm)\TPBi (20 nm)\TPBi:Cs₂CO₃ (5 wt. %, 30 nm)\Al (100 nm), Device-B: ITO/m-MTDATA (40 nm)\NPB(10 nm)\TcTa (10 nm)\TcTa:TPBi:FIRPic (1:1 7 wt. %, 20 nm)\TPBi (20 nm)\TPBi:Cs₂CO₃ (5 wt. %, 30 nm)\m-MTDATA:F4-TCNQ (10 wt. %, 30 nm)\m-MTDATA (20 nm)\NPB (10 nm)\TcTa (10 nm)\TcTa:TPBi:FIRPic (1:1 7 wt. %, 20 nm)\TPBi (20 nm)\TPBi:Cs₂CO₃ (5 wt. %, 20 nm)\Al (100 nm), Device-C: ITO/m-MTDATA (40 nm)\NPB (10 nm)\TcTa (10 nm)\TcTa:TPBi:FIRPic (1:1 7 wt. %, 20 nm)\TPBi (20 nm)\TPBi:Cs₂CO₃ (5 wt. %, 30 nm)\Ag (2 nm)\m-MTDATA:F4-TCNQ (10 wt. %, 30 nm)\m-MTDATA (20 nm)\NPB (10 nm)\TcTa (10 nm)\TcTa:TPBi:FIRPic (1:1 7 wt. %, 20 nm)\TPBi (20 nm)\TPBi:Cs₂CO₃ (5 wt. %, 20 nm)\Al (100 nm), Device-D: ITO/m-MTDATA (40 nm)\NPB (10 nm)\TcTa (10 nm)\TcTa:TPBi:FIRPic (1:1 7 wt. %, 20 nm)\TPBi (20 nm)\TPBi:Cs₂CO₃ (5 wt. %, 30 nm)\Al (2 nm)\m-MTDATA:F4-TCNQ (10 wt. %, 30 nm)\m-MTDATA (20 nm)\NPB (10 nm)\TcTa (10 nm)\TcTa:TPBi:FIRPic (1:1 7 wt. %, 20 nm)\TPBi (20 nm)\TPBi:Cs₂CO₃ (5 wt. %, 20 nm)\Al (100 nm), and Device-E: ITO/m-MTDATA (40 nm)\NPB (10 nm)\TcTa (10 nm)\TcTa:TPBi:Bis(2-phenylquinoline)(acetylacetonate)iridium(III) (Ir(2-phq)₂ acac) (1:1 10 wt. %, 20 nm)\TPBi (20 nm)\TPBi:Cs₂CO₃ (5 wt. %, 30 nm)\Ag (2 nm)\m-MTDATA:F4-TCNQ (10 wt. %, 30 nm)\m-MTDATA (20 nm)\NPB (10 nm)\TcTa (10 nm)\TcTa:TPBi:FIRPic (1:1 7 wt. %, 20 nm)\TPBi (20 nm)\TPBi:

^{a)}Author to whom correspondence should be addressed. Electronic mail: exwsun@ntu.edu.sg.

Cs_2CO_3 (5 wt. %, 20 nm)\Al (100 nm). Device-A is a single emissive unit device. Device-B is the control tandem device with a CGC of TPBi: Cs_2CO_3 m-MTDATA:F4-TCNQ; Device-C and Device-D are the tandem devices with the CGC, respectively, modified by adding an ultrathin Ag and Al layer, respectively, between TPBi: Cs_2CO_3 and m-MTDATA:F4-TCNQ layer, and Device-E is the tandem white device using the same CGC with Device-C. Other used organic materials are NPB, TcTa, FlrPic, Ir(2-phq)₂acac, which are used as hole transport layer, hole transport layer/p-type host, and emitting dopants, respectively. The energy alignment schematic of electrodes and all used materials are shown in Fig. 1.^{16–20}

Patterned ITO-coated glass substrates (15 Ω /sq) were used in our experiment. The ITO substrates were cleaned with de-ionized water, isopropanol, and acetone in sequence first. Then they were oven-dried and treated in O_2 plasma. All functional films and aluminum (Al) electrode were fabricated by thermal evaporation in a single run at a pressure of less than 4×10^{-4} Pa without breaking the vacuum. All the organics and metal oxide were evaporated at a rate of about 0.1–0.2 nm s^{-1} , and the aluminum electrodes were evaporated at a rate of 0.8 nm s^{-1} . A shadow mask was used to define the cathode and to make eight 16 mm^2 devices on each substrate. The luminance-current density-voltage (L-J-V) characteristics and EL spectra were measured simultaneously with a Keithley 2400 power source and a Photoresearch PR 650 spectrometer. The scanning electron microscopy (SEM) was performed using a LEO 1550 Scanning Electron Micrograph on ITO substrate. All UV/Vis/NIR absorption spectra were recorded using a Perkin Elmer Lambda 950 UV/Vis/NIR Spectrophotometer System on quartz substrates. The photoluminescence (PL) decay was measured by a digital phosphor oscilloscope Tektronix DPO 7254 under excitation of a pulsed Nd:YAG fourth harmonic (266 nm) laser with pulse width and repetition rate of 1 ns and 60 Hz. All measurements were carried out at room temperature in ambient atmosphere.

As schemed in Fig. 2(a) inset, the charge generation processes of tandem Device-B take place at m-MTDATA:F4-TCNQTPBi: Cs_2CO_3 interface by electron transfer from the p-type to n-type layer. From Fig. 2(b), the luminous efficiency of tandem Device-B is about two times of that of the single unit Device-A at low current density. If only considering the highest efficiency, the m-MTDATA:F4-TCNQTPBi: Cs_2CO_3 combination can be used as the CGC. But it is noted that the

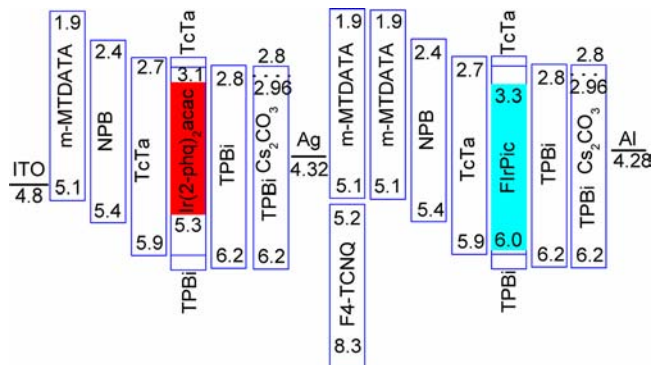


FIG. 1. The schematic of the tandem devices studied.

luminous efficiency of Device-B drops rapidly as the driving current density increases, and the driving voltage of tandem Device-B is much higher than two times of that of the single unit Device-A. Thus, the m-MTDATA:F4-TCNQ/TPBi: Cs_2CO_3 combination is not good enough to play the role of CGC. The CGC actually works as the counterpart of cathode for one emissive unit and anode for another, but even in excellent n-type or p-type doped layers, the free charge carrier concentration ($\sim 10^{19} \text{ cm}^{-3}$) are still several orders of magnitudes less than ITO ($\sim 10^{21} \text{ cm}^{-3}$) or typical metal electrode ($\sim 10^{23} \text{ cm}^{-3}$).^{21,22} Furthermore, the charge carrier binding energy for organic materials is higher than those of ITO and typical metal electrodes. In order to spout enough charges, the tandem Device-B needs much higher external electric field to assist charge generation in CGC, leading to high driving voltage. As current density increases, the m-MTDATA:F4-TCNQ/TPBi: Cs_2CO_3 CGC cannot generate enough charges to balance the opposite charges injected from the both electrodes, leading to charge imbalance in both recombination zones, and ultimately resulting in a lower and fast-dropping luminous efficiency.

Even if the m-MTDATA:F4-TCNQ/TPBi: Cs_2CO_3 combination cannot work as an effective CGC, both the m-MTDATA:F4-TCNQ and TPBi: Cs_2CO_3 are excellent charge injection layers in contact with electrodes.^{6,14,15} Considering the practical handling, transmittance, work function matching, etc., we inserted a 2 nm ultrathin silver film

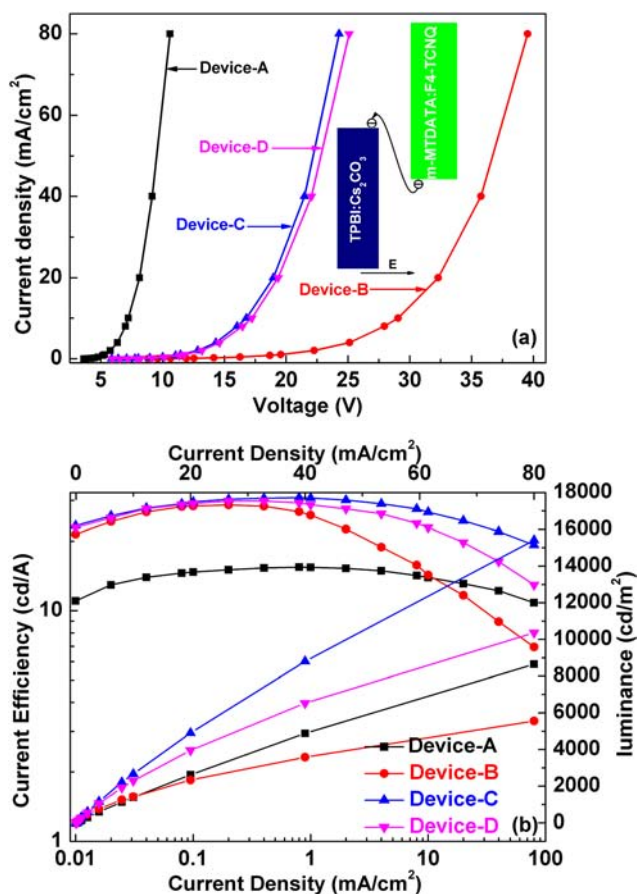


FIG. 2. (a) The current density-driving voltage curves of device-A, B, C, and D. The inset is charge generation process of tandem Device-B under high external electrical field. (b) The luminous efficiency-current density plots of Device-A, B, C, and D.

between m-MTDATA:F4-TCNQ and TPBi:Cs₂CO₃ layers, and fabricated the tandem Device-C. As shown in Fig. 2, comparing to tandem Device-B, the driving voltage of Device-C decreases dramatically to about two times of that of the single unit Device-A, and the luminous efficiency roll-off also improved remarkably in high current density range.

As reported, Ag film mostly works as anode in organic electronic devices, and in some devices with n-type doped electron injection layer, it also can serve as excellent cathode.^{23,24} In tandem Device-C, the Ag thin film, containing a large number of free electrons, should work as anode and cathode simultaneously for the two emissive units. The charge is no longer generated at the m-MTDATA:F4-TCNQ/TPBi:Cs₂CO₃ interface but the Ag ultrathin film and buffer layer interfaces (with m-MTDATA:F4-TCNQ and TPBi:Cs₂CO₃ layers). Comparing to the case of tunneling across the PN junction interface between two organic layers containing a small amount of charges, the charge generation through electron transfer process between Ag ultrathin film and doped organic buffer layers is much easier under external electrical field, which is similar to the process of charge injection from metal electrode into organic layer at the external contacts of the device.

We performed absorption measurements on m-MTDATA:F4-TCNQ (10 wt. %, 30 nm)\TPBi:Cs₂CO₃ (5 wt. %, 30 nm), m-MTDATA:F4-TCNQ (10 wt. %, 30 nm)\Ag (2 nm)\TPBi:Cs₂CO₃ (5 wt. %, 30 nm) films (Fig. 3), and scanning electron microscopy measurement on m-MTDATA:F4-TCNQ (10 wt. %, 30 nm)\Ag (2 nm) film (left inset of Fig. 3). It can be seen from Fig. 3 that the Ag ultrathin film leads to a slightly increased absorbance, which should adversely lower down the ultimate luminous efficiency of the tandem device. However, from the luminous efficiency of tandem Device-C, we see that such negative effect to device overall performance was overwhelmed by the positive effect of more carriers generated. According to the EL spectra of Device-B and -C shown in Fig. 4(b), the microcavity effect in Device-C is negligible.

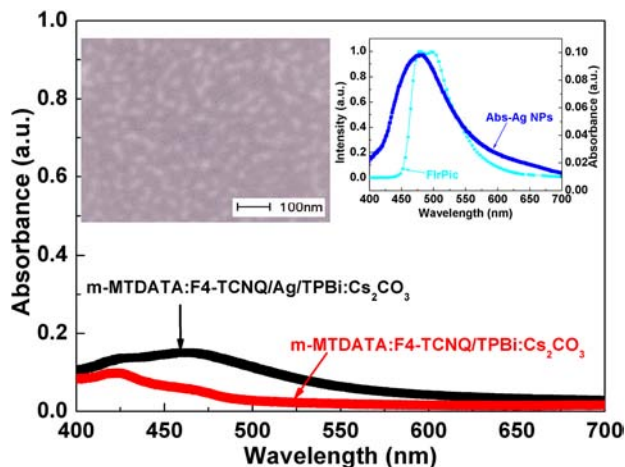


FIG. 3. The absorption of m-MTDATA:F4-TCNQ (10 wt. %, 30 nm)\TPBi:Cs₂CO₃ (5 wt. %, 30 nm) and m-MTDATA:F4-TCNQ (10 wt. %, 30 nm)\Ag (2 nm)\TPBi:Cs₂CO₃ (5 wt. %, 30 nm) films deposited by thermal co-evaporation onto quartz substrate. The inset on the right is the absorption of Ag NP film obtained by subtraction of the two curves above. The inset on the left is the SEM image of m-MTDATA:F4-TCNQ (10 wt. %, 30 nm)\Ag (2 nm) film deposited onto ITO glass substrate. There is a great overlap between absorption spectrum of Ag NPs and emission spectrum of FIrPic dopant.

As presented in the inset of Fig. 3, the Ag ultrathin film deposited on organic film actually exists as nanoparticles (NPs) with a mean size of about 20 nm, which is similar with most reported results of Ag ultrathin film deposited by thermal evaporation method.^{25–27} And such Ag NPs expressed a weak absorption spectrum centered at about 470 nm, originating from the localized surface plasmonic resonance (LSPR) of Ag NPs.^{26–28} The LSPR is actually a resonant photon-induced collective oscillation of valence electrons after photon absorption, which establishes when the frequency of incident photons matches the natural frequency of surface electrons oscillation against the restoring force of positive nuclei.²⁸ When the valence electrons of Ag NPs are agitated, they are more easier to be lost comparing to bulk form of Ag.^{27,28} It is noted that there is a great overlap between the emission spectrum of FIrPic dopant and the absorption spectrum of Ag NPs (right inset of Fig. 3). Thus, Ag NPs can absorb a portion of photons radiated from the recombination zone to excite the LSPR of Ag NPs. And as reported, when the Ag NPs size is less than 30 nm, the surface plasmon can decay through the formation of energetic charge carriers which can transfer to neighboring molecules.²⁸ Additionally, Wu demonstrated that as the size decreases to nanometer scale, the reduction activity of Ag NPs is strengthened.²⁹ Therefore, as described by Fig. 4(a), under external electrical field, in CGC with Ag ultrathin layer, the electron supply for the emissive unit on ITO side becomes better, and the relaxed positive Ag nuclei can receive another electron (i.e., output a hole to) from p-type m-MTDATA:F4-TCNQ layer as the case of metal anode\organic contact.²⁸ Additionally, as the nanoparticle morphology and long distance away from the recombination zone, Ag NPs should not cause any quenching like lithium or cesium.¹¹

To investigate the contribution of LSPR to the charge generation in CGC, we fabricated tandem Device-D, with the ultrathin Ag film replaced by an ultrathin Al film compared to Device C. Al and Ag have similar work function (Fig. 1). As shown in Fig. 5, in Ag (2 nm)\TcTa (10 nm)\TcTa:FIrPic (7%, 5 nm), the phosphorescent lifetime of FIrPic decrease sharply, which should originate from the LSPR of Ag NPs.²⁷ Otherwise we did not observe evidently difference in PL decay curve of Al (2 nm)\TcTa (10 nm)\TcTa:FIrPic (7%, 5 nm), which means the photon radiated from FIrPic emitter

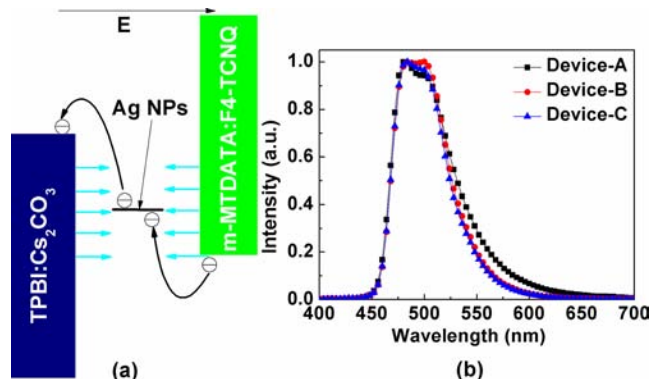


FIG. 4. The charge generation process of tandem Device-C under external electrical field (a). The electroluminescence spectra of all devices at 1 mA/cm² (b). The spectra of tandem Device-B and Device-C are similar, meaning there is no microcavity effect caused by Ag NPs layer.

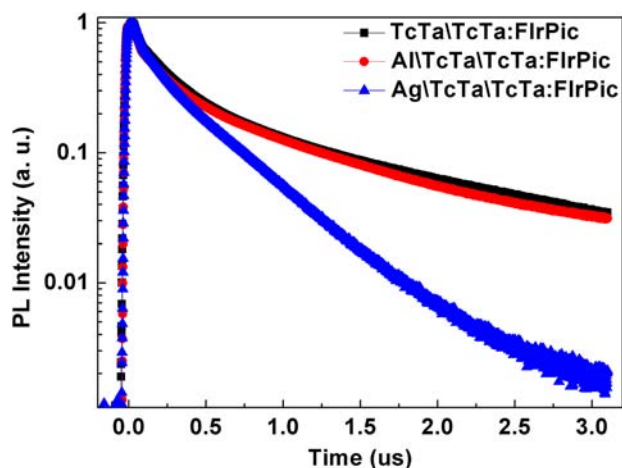


FIG. 5. The photoluminescence decay curves of TcTa (10 nm)\TcTa:FIRPic (7%, 5 nm), Al (2 nm)\TcTa (10 nm)\TcTa:FIRPic (7%, 5 nm), and Ag (2 nm)\TcTa (10 nm)\TcTa:FIRPic (7%, 5 nm) deposited onto quartz substrates by thermal evaporation.

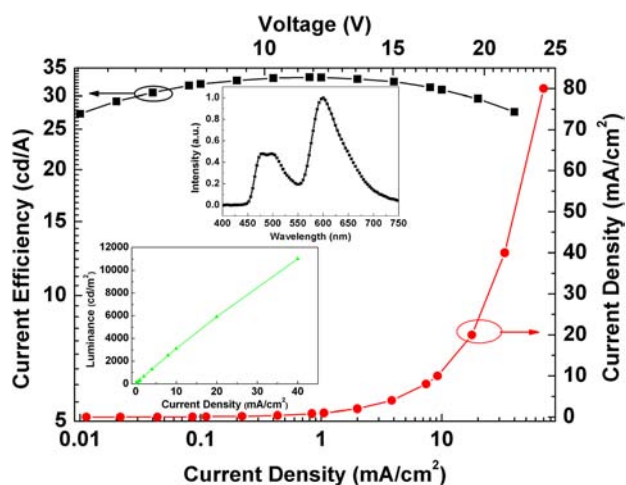


FIG. 6. The current density-driving voltage curves and luminous efficiency-current density plots of white Device-E. The inset is the luminance plots and emission spectrum.

can hardly excite LSPR for Al ultrathin film. As seen in Fig. 2, both driving voltage and luminous efficiency of Device-D is close to those of Device-C in low driving current density, but as the driving current density increases, the driving voltage goes up slightly and the luminous efficiency drops. As luminance increases, the role of LSPR generated by Ag NPs in Device-C strengthened, and the CGC generates more charges with lower driving voltage comparing to Device-D with merely no LSPR. Furthermore, we fabricated an efficient tandem white OLED Device-E using the same CGC as Device-C, which showed reasonable good performance (Fig. 6).

In conclusion, by inserting an ultrathin Ag NPs layer at the interface between p-type layer (m-MTDATA:F4-TCNQ) and n-type layer (TPBi:Cs₂CO₃), the tandem device performance was improved dramatically. In the CGC with Ag NPs, the charge generation process is different from that of

organic PN junction. Additionally, due to the great overlap between Ag NPs LSPR absorption and FIRPic dopant emission spectra, the LSPR also contribute to the tandem device performance.

This work was financed by the Science and Engineering Research Council, Agency for Science, Technology and Research (A*STAR) of Singapore (Project Nos. 092 101 0057 and 092 151 0088), and National Research Foundation (Grant Nos. NRF-RF-2009-09 and NRF-CRP-6-2010-2). The work was also supported by the National Natural Science Foundation of China (NSFC) (Project Nos. 61006037 and 61076015).

- ¹W. Staroske, M. Pfeiffer, K. Leo, and M. Hoffmann, *Phys. Rev. Lett.* **98**, 197402 (2007).
- ²M. A. Baldo, C. Adachi, and S. R. Forrest, *Phys. Rev. B* **62**, 10967 (2000).
- ³P. Cusumano, F. Buttitta, A. Di Cristofalo, and C. Cali, *Synth. Met.* **139**, 657–661 (2003).
- ⁴S. Reineke, F. Lindner, G. Schwartz, N. Seidler, K. Walzer, B. Lössem, and K. Leo, *Nature* **459**, 234 (2009).
- ⁵L. Li, M. Guan, G. H. Cao, Y. Y. Li, and Y. P. Zeng, *Solid State Commun.* **150**, 1683–1685 (2010).
- ⁶C. W. Chen, Y. J. Lu, C. C. Wu, H. E. Wu, C. W. Chu, and Y. Yang, *Appl. Phys. Lett.* **87**, 241121 (2005).
- ⁷M. Kröger, S. Hamwi, J. Meyer, T. Dobbertin, T. Riedl, W. Kowalsky, and H. Johannes, *Phys. Rev. B* **75**, 235321 (2007).
- ⁸Q. Y. Bao, J. P. Yang, J. X. Tang, Y. Li, C. S. Lee, and S. T. Lee, *Org. Electron.* **11**, 1578–1583 (2010).
- ⁹L. S. Liao, W. K. Slusarek, T. K. Hatwar, M. L. Ricks, and D. L. Comfort, *Adv. Mater.* **20**, 324–329 (2008).
- ¹⁰X. F. Qi, N. Li, and S. R. Forrest, *J. Appl. Phys.* **107**, 014514 (2010).
- ¹¹I. W. Wu, C. L. Chuang, P. S. Wang, W. H. Tseng, and C. I. Wu, *Appl. Phys. Lett.* **100**, 173302 (2012).
- ¹²T. W. Lee, T. Noh, B. K. Choi, M. S. Kim, D. W. Shin, and J. Kido, *Appl. Phys. Lett.* **92**, 043301 (2008).
- ¹³Y. Cai, H. X. Wei, J. Li, Q. Y. Bao, X. Zhao, S. T. Lee, Y. Q. Li, and J. X. Tang, *Appl. Phys. Lett.* **98**, 113304 (2011).
- ¹⁴C. W. Law, K. M. Lau, M. K. Fung, M. Y. Chan, F. L. Wong, C. S. Lee, and S. T. Lee, *Appl. Phys. Lett.* **89**, 133511 (2006).
- ¹⁵M. H. Ho, T. M. Chen, P. C. Yeh, S. W. Hwang, and C. H. Chen, *Appl. Phys. Lett.* **91**, 233507 (2007).
- ¹⁶H. Liu, F. Yan, H. Wang, Y. Miao, X. Du, S. Jing, Z. Gao, L. Chen, Y. Hao, and B. Xu, *Appl. Phys. Lett.* **102**, 013304 (2013).
- ¹⁷N. Ishiyama, M. Kubo, T. Kaji, and M. Hiramoto, *Appl. Phys. Lett.* **101**, 233303 (2012).
- ¹⁸F. Yan, H. Liu, W. Li, B. Chu, Z. Su, G. Zhang, Y. Chen, J. Zhu, D. Yang, and J. Wang, *Appl. Phys. Lett.* **95**, 253308 (2009).
- ¹⁹N. Matsusue, Y. Suzuki, and H. Naito, *Jpn. J. Appl. Phys., Part 1* **44**, 3691 (2005).
- ²⁰W. Jeon, T. Park, and J. Kwon, *J. Inf. Disp.* **10**, 87 (2009).
- ²¹B. L. Anderson and R. L. Anderson, *Fundamentals of Semiconductor Devices* (McGraw-Hill, New York, 2004).
- ²²S. Franzen, *J. Phys. Chem. C* **112**, 6027–6032 (2008).
- ²³C. W. Chen, P. Y. Hsieh, H. H. Chiang, C. L. Lin, H. M. Wu, and C. C. Wu, *Appl. Phys. Lett.* **83**, 5127 (2003).
- ²⁴M. Thomschke, S. Hofmann, S. Olthof, M. Anderson, H. Kleemann, M. Schober, B. Lössem, and K. Leo, *Appl. Phys. Lett.* **98**, 083304 (2011).
- ²⁵B. Niesen, B. P. Rand, P. V. Dorpe, H. Shen, B. Maes, J. Genoe, and P. Heremans, *Opt. Express* **18**, 19032–19038 (2010).
- ²⁶P. L. Redmond, A. J. Hallock, and L. E. Brus, *Nano Lett.* **5**, 131–135 (2005).
- ²⁷F. Yan and X. W. Sun, *Appl. Phys. Lett.* **102**, 043303 (2013).
- ²⁸S. Linic, P. Christopher, and D. B. Ingram, *Nature Mater.* **10**, 911–921 (2011).
- ²⁹Z. Wu, *Angew. Chem., Int. Ed.* **51**, 2934–2938 (2012).